The formation and evolution of Ni_2Cr precipitates in Ni-Cr model alloys as a function of stoichiometry characterized by synchrotron x-ray diffraction

*N. Aerne[1], D. Sprouster[2], J. D. Tucker[1, *]*

[1] School of Mechanical, Industrial and Manufacturing Engineering, Oregon State University, Corvallis, OR 97331, USA

[2] Department of Materials Science and Chemical Engineering, Stony Brook University, Stony Brook, NY 11794, USA

[*] Julie.Tucker@oregonstate.edu

Abstract

Ni-based alloys containing significant amounts of Cr, may precipitate new phases during long-term service at elevated temperatures. In Ni-Cr model alloys, the formation of Ni_2Cr has been found to impact the material properties, including the strength and ductility after isothermal aging below the critical temperature of 590 °C. In this work, we quantify the formation and evolution of long-range ordering in four Ni-Cr binary model alloys (Ni/Cr = 1.8, 2.0, 2.2, 2.4) after isothermal aging up to 10,000 h at temperatures between 373-475 °C. The alloys were characterized by hardness testing and synchrotron-based x-ray diffraction to quantify the impact of Ni_2Cr phase fraction and precipitate size on mechanical properties. After 500 h of isothermal aging, the formation of Ni_2Cr was detected in all four alloys at 475 °C. In the stochiometric alloy samples (Ni/Cr = 2.0), the formation of Ni_2Cr was found after 500 and 3,000 h aging at 418 and 373 °C, respectively. We found that the matrix lattice contraction and Ni_2Cr phase fraction both saturate after early aging times. This is in stark contrast to the hardness and Ni_2Cr precipitate size that both continue to increase with increasing aging time. Our results highlight that changes in hardness correlate linearly with Ni_2Cr precipitate size rather than phase fraction. This important structure-property relationship can potentially help define Ni-Cr-based component lifetimes directly through an understanding of how Ni_2Cr formation impacts strength and ductility. We find that a precipitation hardening model for critical resolved shear stress with weakly coupled dislocations shows good agreement with the material property changes quantified from experimental measurements.

Keywords: *Nickel alloys, Long-range ordering, Hardness, Synchrotron diffraction, Precipitation strengthening, Critical resolved shear stress*

1. Introduction

Ni-based superalloys are well known for their excellent material properties and are frequently selected for industrial applications with elevated temperatures, corrosive environments, high strength, and/or fracture toughness service requirements. The performance and development of Ni-based superalloys and their model alloy counterparts has been the focus of an extensive amount of research [1]–[14]. Changes in Ni-based superalloys microstructure from exposure to service environments are therefore of interest to the global community. In the nuclear industry, interest in the long-range order (LRO) Ni_2Cr phase formation has been motivated by service conditions (i.e., elevated service temperatures and harsh environments) for decades [15]–[17]. Commercial alloy 690 (58-62 wt. % Ni, 27-31 wt. % Cr, 7-11 wt. % Fe) has been investigated with respect to Ni_2Cr formation to understand the potential impacts on use as a structural component material in pressurized water reactors [8]–[10]. Previous research focused on the Fe content to bridge understanding from model to commercial alloys [9], [11], [13]. Here in our research we focus on the compositional differences in a series of four Ni-Cr binary model alloys (Ni/Cr = 1.8, 2.0, 2.2, 2.4) to understand differences in stoichiometry as they relate to the precipitate nucleation and growth and mechanical behavior.

Ni_2Cr phase formation in Ni-Cr alloys occur at temperatures below 590 °C [3]. In isothermal aging experiments of model Ni-Cr alloys near the Ni_2Cr stoichiometry (Ni/Cr = 2.0), Ni_2Cr phase formation results in an increase in hardness [4], [9], [10], contraction of the face-centered cubic (FCC) lattice parameter [10], [11], and degradation in ductility [9], [10] and susceptible to stress corrosion cracking with a peak transformation rate near 475 °C [9], [18]. However, the degree of Ni_2Cr phase formation and the rate of the transformation, responsible for the changes in material properties are yet to be comprehensively addressed with respect to the Ni and Cr composition. Furthermore, the phase boundary for Ni_2Cr formation is poorly defined below 450 °C in the Ni-Cr binary system due to lack of experimental data. Most recent efforts show the Ni_2Cr boundary, as defined with CALPHAD method, displays a peritectoid reaction that narrows sharply toward stoichiometric compositions at low temperatures [3].

One common way to model the ordering kinetics in Ni-Cr alloys, as functions of time and temperature, is the utilization of the Arrhenius form of the Kolmogorov-Johnson-Mehl-Avrami (KJMA) equation, which has been widely used in previous studies [4], [8], [9], [13], [19]–[24]. The KJMA equations have been fit to changes in material behavior, where the change in behavior is assumed to be equivalent to the transformed fraction of Ni_2Cr or ordered material. Changes in hardness [4], [8], [9], [11], electrical resistivity [8], [13], and FCC lattice parameters [4], [11] have been analyzed with the KJMA method to estimate the activation energy, and formation characteristics of Ni_2Cr in various Ni-based alloys. A limitation of using this method is that the amount of material transformed is an assumed value, and changes in the microstructure and mechanisms for nucleation and growth are not directly accessed. Therefore, it is critical to investigate the actual phase fraction of Ni_2Cr to align Ni-based component lifetime predictions with real material responses to their respective service conditions and environments.

Quantifying the phase fraction of Ni_2Cr presents a number of challenges depending on the technique employed. Transmission electron microscopy (TEM), atom probe tomography (APT), and X-ray diffraction (XRD) are all capable in determining the phase fraction. However, TEM and APT both examine limited amounts of material making the phase fraction of Ni_2Cr difficult to determine from these techniques and requires extensive effort with large systematic studies. Additionally, the poor contrast between Ni and Cr (*e.g.,* similarities in atomic number) adds to the complexity of this task, particularly for APT where the boundary of Ni_2Cr is difficult to distinguish due also to the limited compositional difference between the fully coherent Ni_2Cr phase and the Ni-Cr matrix [14]. With TEM, Ni_2Cr precipitates can only be viewed in a few crystallographic equivalent variants [1], [4], [5], which makes finding precipitates at early nucleation

times from thermal aging particularly cumbersome and highly dependent on the grain orientation and tilt range. Furthermore, the LRO phase is not visible in bright field TEM. The only way to image it is using dark field imaging by selecting the secondary diffraction pattern of LRO only. Contrast of the image is poor due to the described difficulties, which makes the phase fraction measurements to be imprecise. Phase fractions of Ni_2Cr with TEM and APT can be determined directly from 2D images (TEM) and 3D volumes (APT). In contrast, XRD determines the phase fraction from a structural refinement from experimental patterns. Here the advantage of XRD over TEM and APT lies in the amount of material probed (TEM: < 10^{-8} mm^3, XRD: ~0.5 mm^3). Therefore, synchrotron-based XRD offers a comprehensive and rapid means to identify and determine the phase fraction for large systematic studies [4], [12], [14] due to the large sampling volumes and sensitivity to minor precipitate populations stemming from high flux available at synchrotron sources. Additionally, transmission-mode geometry available with synchrotron XRD allows for excellent measurement of average global material properties and would minimize the impact of any potential residual stress in samples from thermal gradients present in material processing and/or in sample preparation.

The purpose of this research is to quantify the structure-property relationship of Ni_2Cr phase formation and growth in a series of Ni-Cr binary alloys as functions of aging time, temperature, and composition. The evolution in microstructure and mechanical properties were determined from synchrotron-based XRD and Vickers microhardness testing, respectively. Four Ni-Cr binary model alloys (Ni/Cr = 1.8, 2.0, 2.2, 2.4) were investigated following isothermal aging campaigns at three temperatures (373, 418, and 475 °C) for up to 10,000 h. The evolution of the microstructure including the phase fraction, lattice parameters, and size of Ni_2Cr ordered precipitates were determined through refinement and correlated with hardness data. These efforts serve to aid Ni-based alloy service life predictions at elevated temperatures by understanding the formation of Ni_2Cr and mechanical property impacts in Ni-Cr model alloys from isothermal aging campaigns for long exposure periods.

2. Experimental Methods

2.1. *Model alloys*

The Ni-Cr binary model alloys were fabricated via arc-melting to create buttons of ~300 g. The buttons were re-melted three times, homogenized in a furnace for 24 h at 1093 °C, hot rolled into plates and water quenched to room temperature. Individual buttons were prepared with different stoichiometries for Ni/Cr atomic ratios from 1.8 to 2.4. The compositions of these alloys are given in Table 1. The rolled plates were cut into 10×10×5 mm^3 samples via electrical discharge machining. The samples were then isothermally aged in air in box type furnaces at temperatures of 373, 418, and 475 °C and aging times: 500, 1,000, 3,000, 5,000, and 10,000 h, and water quenched to room temperature. Additional details on the chemical analysis, temperature monitoring and calibration can be found in ref. [4]. The isothermal aging temperatures were maintained at ±5 °C of target temperatures, and the time accrued for aging campaigns are estimated to be ±1 % of target times.

Table 1. Chemical composition (wt.%) of alloys investigated

Alloy Name	Ni-Cr Atomic ratio	Ni	Cr	P	S	C	other*
Ni-Cr 1.8	1.80	67.30	32.65	0.007	0.002	0.01	<0.005
Ni-Cr 2.0	2.01	69.36	30.62	0.006	0.002	0.01	<0.005
Ni-Cr 2.2	2.21	71.40	28.58	0.006	0.002	0.01	<0.005
Ni-Cr 2.4	2.35	72.58	27.36	0.006	0.001	0.01	<0.005

other*- Fe, Mo, Nb+Ta, Co, Mn, Si, Cu, Al, Ti, Mg, B, Ca

2.2. Hardness testing

The microhardness testing was performed on flat surfaces of the bulk samples. The surface finish for testing was achieved with wet polishing on standard 8-inch polishing wheels using SiC papers from 240 to 1,200 grit, and then using alumina polishing solutions from 1 μm to 0.05 μm on felt polishing cloths. Vickers hardness measurements were performed by using a Leco 400 A Hardness Tester with pyramidal diamond tip and a load of 500 gf (or 4.9 N) applied for 15 s. A M55x objective lens with a 0.65 numerical aperture were used to measure the diagonal of the residual imprint. Ten indentations were performed in independent locations on each sample, following statistical analysis suggestions of Vickers Hardness research [25]. The average standard deviation of Vickers hardness values for all samples was ±8.5 HV.

2.3. *X-ray diffraction (XRD)*

Samples for the XRD measurements were cut from the bulk samples and mechanically polished to 5 × 5 × 0.1 mm^3 in size. XRD measurements were performed at the X-ray Powder Diffraction beamline 28-ID-2 [26], [27] at the National Synchrotron Light Source II. All samples were measured in transmission-mode geometry with an amorphous silicon-based flat panel detector (Perkin-Elmer). The sample-to-detector distance was calculated to be 1420.16 mm. The incident wavelength and of the x-ray beam was 0.1875 Å (66.11 keV). The samples were rotated during measurements to improve the powder averaging. Typical count times for each sample were 10 s. The sample-to-detector distance, tilts of the detector relative to the beam were determined using a NIST standard reference material 660c, LaB_6 powder standard. The two-

dimensional detector images were radially integrated, and background subtracted to obtain powder diffraction patterns. These operations were completed with the NIKA and IRENA programs [28], [29]. Refinements on the one-dimensional powder diffraction patterns were performed in MAUD [30]. The XRD peak profiles were modeled using a modified pseudo-Voigt function. The instrument contribution to the broadening of the measured profiles was quantified by fitting the LaB_6 powder standard, with known crystalline-domain size and negligible strain contribution. The Gaussian and Lorentzian-based broadening parameters were subsequently fixed during the analysis of the alloys under investigation. The volume fractions, precipitate sizes, and lattice parameters were allowed to vary during the Rietveld refinements for the FCC matrix and Ni_2Cr ($MoPt_2$ -type crystal structure). The precipitate size was refined with the Scherrer formula, shown in equation (1), where d is the precipitate size, K is a constant based on the geometry of the crystallography, λ is the wavelength, ω is the width, and θ is the angle of the Bragg reflection [31], [32]. The quantitative phase analysis performed to determine the phase fraction uses the Hill and Howard (ZMV) approach shown in equation (2), where W_p is the weight fraction of phase p, S_p is the Rietveld scale factor, Z is the number of formula units per unit cell, M is the mass of the unit cell, and V is the unit-cell volume [31], [33]. The lattice parameters were determined with the standard application and refinement of Bragg's law based on the peak location and intensity, where a known crystal structure is fit to the refined inter atomic spacing [34]. The microstrain parameter was allowed to refine for the FCC host only (thus, the refined precipitate size parameters are lower limits for the Ni_2Cr phase). These operations performed within MAUD.

$$d = \frac{K\,\lambda}{\omega \cos\theta} \tag{1}$$

$$W_p = \frac{S_p(ZMV)_p}{\sum_i S_i(ZMV)_i} \tag{2}$$

Table 2 shows the test matrix for XRD characterization. Previous alloys from ref. [4] are also shown in Table 2 to clarify the added contributions in this work. To quantify the evolution of Ni_2Cr at lower temperatures, a series of (Ni/Cr = 2.0) samples aged at 373, 418 and 475 °C, up to 10,000 h were investigated. To understand the evolution of Ni_2Cr as a function of stoichiometry, off-stoichiometric Ni/Cr = 1.8, 2.2 and 2.4 samples were investigated after aging at 475 °C, near the peak transformation temperature.

Table 2. Test matrix for XRD. Tested stoichiometry is shown in each table cell.

Temperature	Isothermal Aging Time (h)				
(°C)	500	1000	3000	5000	10,000
373	2.0	2.0	2.0	2.0	(2.0)*
418	2.0	2.0	2.0	2.0	(2.0)*
475	1.8, 2.0, 2.2, 2.4 (2.0)*	1.8, 2.0, 2.2, 2.4 (2.0)*	2.2, 2.4 (2.0)*	1.8, 2.2, 2.4 (2.0)*	1.8, 2.2 (1.8, 2.0, 2.2, 2.4)*

* - Preformed previously in Teng et al. [4]

*3. **Results and Discussion***

The XRD results are presented in four sections to systematically describe the experiment: (3.1) the qualitative behavior of the XRD patterns, (3.2) the quantitative microstructural results from XRD refinements and hardness results to explore the role of stoichiometry in Ni-Cr model alloys, (3.3) the quantitative microstructural results and hardness results for the (Ni/Cr = 2.0) samples after aging campaigns

at 373, 418, and 475 °C, and finally (3.4) correlating the Ni_2Cr precipitate sizes and increase in hardness determined for all samples investigated.

3.1. Qualitative XRD analysis

The XRD patterns for the Ni-Cr model alloys investigated here are shown in this section. Figure 1 shows XRD patterns for the (Ni/Cr = 2.0) samples after (a) 500 h and (b) 10,000 h aging at 373, 418 and 475 ºC. An as received (AR) Ni/Cr=2.0 sample is also shown in Figure 1 (b) for reference. Figure 1 also shows the XRD patterns for the different Ni-Cr stoichiometries investigated after (c) 500 h and (d) 10,000 h aging at 475 ºC. The patterns are offset from one another to show multiple samples on a single plot. The XRD data from ref. [4] are also included in (b) and (d) for completeness (peak positions are slightly shifted due to the smaller wavelength used in ref. [4]). All samples show dominant FCC matrix peaks. No body-centered cubic Cr peaks were detected. The body-centered orthorhombic phase Ni_2Cr, commonly referred to as $MoPt_2$, are observable as low angle peaks in (a)-(d). All four stoichiometries confirm the formation of Ni_2Cr with peaks after 500 h at 475 °C. At lower temperatures, the (Ni/Cr = 2.0) sample aged at 418 °C also shows Ni_2Cr diffraction peaks after 500 h whereas the (Ni/Cr = 2.0) sample aged to 500 h at 373 °C does not. The Ni_2Cr diffraction peaks are visible after 3000 h for this sample. The XRD peaks for the Ni_2Cr phase vary in intensity and width across the different stoichiometry, time, and temperatures investigated, indicating differences in precipitate size. The Ni_2Cr peak intensity generally increases and the full width at half maximum decrease with continued aging time regardless of composition. As plots (a) and (b) show for the (Ni/Cr=2.0) samples, the increasing intensity and decreasing width of the Ni_2Cr peaks closely follow the aging temperate with 475 > 418 > 373 °C. XRD peak broadening of Ni_2Cr at lower temperatures has previously been observed [4]. In addition, Gwalani et al. show in their Ni-33Cr At. % model alloy aged at 475 °C that Ni_2Cr diffraction peaks are observed after 240 h with synchrotron-based XRD[14]. Likewise, Verma et al. show in their Ni-32Cr At. % model alloy aged at 500 °C that Ni_2Cr peaks are observed after 1000 h with neutron diffraction [12].

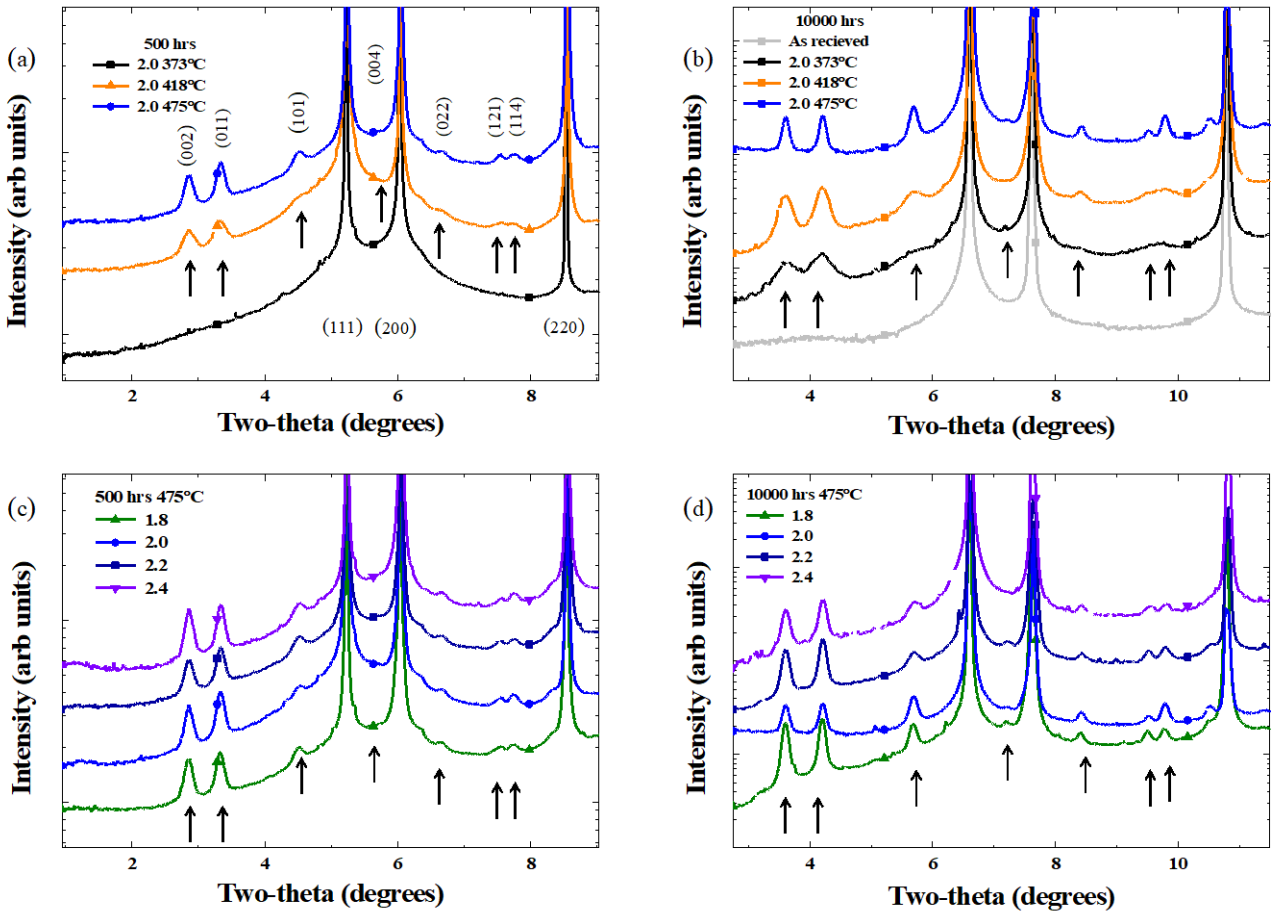

Figure 1. Synchrotron XRD of Ni-Cr model alloys showing(a) Ni/Cr=2.0 after 500 h at 373, 418, and 475 °C, (b) Ni/Cr=2.0 after 10,000 h at 373, 418, 475 °C and in as received sample, (c) all alloys after aging 500 h at 475 °C and (d) all alloys after aging 10,000 h at 475 °C. Note that, arrows and vertical miller indices indicate distinct Ni_2Cr phase peaks, other peaks are associated with the FCC matrix phase and have horizontal miller indices, and that the patterns are offset to show similar aging times on the same plot.

3.2. Role of stoichiometry at isothermal aging temperature 475 °C

The quantitative XRD and hardness results for all stoichiometries isothermally aged at 475 °C are presented in this section. Figure 2 shows the quantitative XRD results, including: (a) the change in FCC lattice parameter, (b) Ni_2Cr precipitate size, (c) phase fractions of the Ni_2Cr phase, and (d) hardness for the four Ni-Cr alloys (Ni/Cr = 1.8, 2.0, 2.2, and 2.4) isothermally aged at 475 °C for up to 10,000 h. Figure 2 shows that after 500 h of isothermal aging at 475 °C, Ni_2Cr is detected and results in appreciable changes in both the microstructure and hardness. The microstructural results, including lattice parameter, phase fraction, and precipitate size from the XRD refinements, are listed in Table 3.

The lattice parameter in the as received condition from the alloys vary and are dependent on the composition of Ni and Cr. The lattice parameters increase with Cr content such that stoichiometry 1.8 > 2.0 > 2.2 > 2.4

in agreement with Vegard's law and past works [35], [36]. A lattice contraction is quantified for all stoichiometries with isothermal aging at 475 °C. The largest contractions occur in alloy compositions close to stoichiometric conditions (*i.e.,* 2.0 > 1.8 ≥ 2.2 > 2.4). The overall contraction agrees with previous findings [4], [10], [11], [14], [37], that report -0.25% lattice contraction in (Ni/Cr = 2.0) alloys. The trend in contraction shows that at 475°C, the majority of the lattice contraction occurs within the first 1,000 h, and then plateaus. The lattice contraction from ref. [14] for a single Ni-Cr model alloy (Ni/Cr = 2.03) are also shown in Figure 2 (a) for comparison. Gwalani et al. show the majority of the lattice contraction happens between 90 and 240 h for near stoichiometric samples at isothermal aging temperature 475 °C. It is worth noting the average reported grain size in ref. [14] was ~25 μm, compared to ~150 μm in the present research.

In Figure 2 (b), the Ni_2Cr precipitate size determined from the XRD analysis is shown for all stoichiometries after isothermal aging up to 10,000 h at 475 °C. After 500 h, Ni_2Cr precipitates have already nucleated with sizes in the range of 8-10 nm (depending on stoichiometry). With increasing aging time, the Ni_2Cr precipitates increase in size with the (Ni/Cr = 2.0) having the largest Ni_2Cr precipitates (19 nm), and still possibly increasing. The Ni_2Cr precipitate size in the off-stoichiometric conditions range from 13-15 nm and appear to have plateau after 1,000 h of aging. The sizes reported here agree with previous TEM observations of Ni_2Cr cluster for sample at 475 °C [4]. Gwalani et al. and Verma et al. do not report Ni_2Cr size in the refinements of their Ni-Cr model alloy [12], [14].

Figure 2 (c) shows the trends in the phase fractions of Ni_2Cr for all stoichiometries. Interestingly, the phase fraction of Ni_2Cr reaches a maximum value after 500 h for all stoichiometries and appears to plateau at a value of 9 %. In similar Ni-Cr model alloys near stoichiometric compositions there is contrasting data in the literature, where APT findings of volume fraction are <5 % from isothermal aging at 475 °C between 90 and 8,000 h, while neutron diffraction refinement places volume fractions around 40 % from isothermal aging at 500 °C for 1,000 h [12], [14]. It is worth mentioning that previous synchrotron-based XRD experiments did not quantify phase fractions but focused on lattice parameters derived from in-situ experiments [14]. In commercial alloys, TEM observations from proton irradiation experiments, *e.g.* in alloy 625 indicate volume fractions of 7 % [1]. Additionally, when comparing the XRD patterns from previous research [12], [14] and our current results, despite differences in reported phase fraction, the relative peak intensities from Ni_2Cr peaks are comparable. We propose that due to the large test matrix employed in our research that contain numerous samples showing clear observations of Ni_2Cr peaks, >20 samples, versus 3 [14], versus 2 [12], that the phase fraction reported here reflects the most up to date values for Ni_2Cr in Ni-Cr-based alloys.

Figure 2 (d) shows the evolution of hardness from the Vickers indentation campaign for the four stoichiometries investigated after isothermal aging at 475 °C. All Ni-Cr stoichiometries show an increase in hardness with time, with rapid increases in hardness after 1,000 h. At longer aging times the hardness continues to increase in value. The (Ni/Cr = 2.0) samples show a greater increase in indentation hardness when compared to the off-stoichiometric alloy (Ni/Cr = 1.8, 2.2, and 2.4) samples. The change in hardness and starting Vickers hardness number shows good agreement with previous literature [9], [12].

There is a clear correlation between the indentation hardness and the ordered precipitate size (*i.e.,* plots (d) and (b)). This correlation is explored further in section (3.4). It is worth noting that there does not appear to be a strong correlation between the phase fractions determined from the XRD analysis and the indentation hardness. More specifically, the phase fractions saturate after 1,000 h, while the hardness continues to increase with further aging time. This is evidence that the change in hardness is less dependent on the amount of Ni_2Cr present, and more correlated to the Ni_2Cr precipitate size. The change in the FCC matrix lattice parameters and phase fraction of Ni_2Cr do appear to be correlated, potentially due to the depletion

of Cr from the matrix needed to form Ni_2Cr precipitates but may also be due to the change in volume between the matrix and precipitate. It is an open question if the indentation hardness and precipitate size have indeed reached saturation, requiring further isothermal aging beyond 10,000 h investigated in this research.

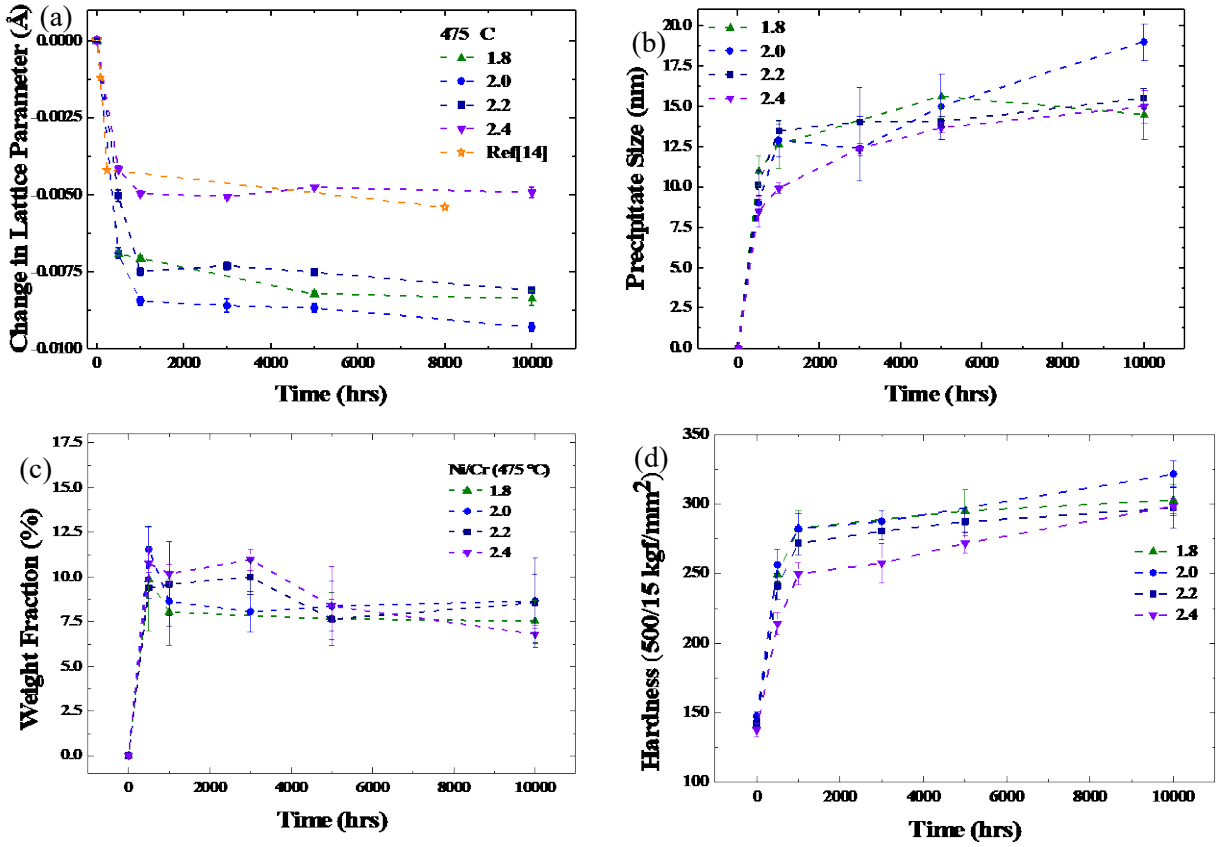

Figure 2. Quantitative XRD and hardness results for the four Ni-Cr alloys as a function of time after aging at 475 °C: (a) Change in FCC matrix lattice parameter; (b) the Ni_2Cr ordered precipitate size; (c) phase fraction of Ni_2Cr phase; (d) Vickers indentation hardness.

Table 3. Summary of Rietveld refinements on Ni-Cr model alloys.

Ni/Cr Ratio	Temp °C	Time h	Lattice parameter Å ±	Phase fraction Ni_2Cr (%) ±	Precipitate- size nm ±
2.0	373	500	3.56598 (0.00003)	- -	- -
		1000	3.56402 (0.00002)	- -	- -
		3000	3.56228 (0.00003)	10.7 (4.8)	4.3 (0.4)
		5000	3.56164 (0.00002)	10.4 (2.3)	4.8 (0.4)
*		10000	3.56158 (0.00010)	6.6 (0.2)	4.0 (1.0)
2.0	418	500	3.55852 (0.00003)	16.3 (2.8)	4.6 (0.3)
		1000	3.55974 (0.00003)	13.7 (1.2)	5.4 (0.5)
		3000	3.56008 (0.00003)	11.4 (3.0)	7.0 (1.1)
		5000	3.55890 (0.00003)	11.6 (3.0)	8.7 (0.7)
*		10000	3.55954 (0.00010)	9.5 (0.3)	6.7 (1.0)
1.8		AR	3.57068 (0.00010)		
1.8	475	500	3.56299 (0.00002)	9.9 (2.9)	11.0 (0.9)
		1000	3.56284 (0.00003)	8.0 (1.9)	12.6 (1.3)
		5000	3.56167 (0.00003)	7.7 (1.5)	15.6 (1.3)
		10000	3.56231 (0.00004)	7.5 (1.2)	14.5 (1.5)
2.0		AR	3.56721 (0.00005)		
2.0	475	500	3.56031 (0.00002)	8.0 (1.0)	10.4 (0.7)
		1000	3.55875 (0.00002)	8.8 (0.7)	12.6 (0.4)
		3000	3.55861 (0.00003)	8.0 (1.1)	12.4 (0.2)
		5000	3.55853 (0.00002)	8.3 (1.4)	15.0 (0.2)
*		10000	3.55791 (0.00003)	8.6 (1.5)	19.0 (1.1)
2.2		AR	3.56368 (0.00005)		
2.2	475	500	3.55824 (0.00013)	9.4 (0.6)	10.2 (0.8)
		1000	3.55577 (0.00008)	9.6 (2.4)	13.5 (0.6)
		3000	3.55596 (0.00007)	10.0 (0.9)	14.0 (0.5)
		5000	3.55470 (0.00006)	7.6 (1.1)	14.1 (0.3)
		10000	3.55558 (0.00009)	8.6 (2.5)	15.5 (0.6)
2.4		AR	3.55963 (0.00004)		
2.4	475	500	3.55547 (0.00003)	10.8 (0.9)	8.5 (0.9)
		1000	3.55467 (0.00003)	10.2 (0.5)	9.9 (0.3)
		3000	3.55457 (0.00003)	10.9 (0.6)	12.4 (0.3)
		5000	3.55488 (0.00003)	8.4 (2.2)	13.7 (0.3)
*		10000	3.55470 (0.00003)	6.8 (0.5)	15.0 (0.4)

* - Teng, et al. – Data was analyzed and refined again or directly from ref. [4]

3.3. Temperature-dependent evolution for the Ni/Cr = 2.0 samples

The quantitative XRD and hardness results for stoichiometric (Ni/Cr = 2.0) alloys aged at different temperatures are presented in this section. The alloys were isothermally aged at 373, 418, and 475 °C for up to 10,000 h to determine the effects of temperature on the evolution of Ni_2Cr. Figure 3 shows the quantitative XRD results, including in plot (a) the change in FCC lattice parameter, (b) Ni_2Cr precipitate size, (c) phase fractions of the Ni_2Cr phase, and (d) Vickers hardness. The formation of Ni_2Cr precipitates is clearly observed after 500 h of aging at 418 °C and 475 °C. At 373 °C, Ni_2Cr precipitates were not observed until after 3,000 h of aging. Figures in the supplemental results show the synchrotron-based XRD evolution of (Ni/Cr=2.0) samples at 373 and 418 °C to aid the identification of Ni_2Cr phase from our experiments. The quantitative XRD results for this section are also given in Table 3.

Figure 3 (a) shows the change in FCC matrix lattice parameter as a function of aging temperature and time. Like the results in section (3.2), the FCC matrix contracts upon aging at all temperatures, and the amount of contraction increases with aging temperature (*i.e.,* 475 > 418 > 373 °C). The contraction for the 418 and 475 °C temperatures show that lattice contraction plateaus after 1,000 h. For the 373 °C isothermal aging temperature, lattice contraction plateaus after 3,000 h. However, whether or not these lower temperatures have reached true saturation would require further aging past 10,000 h. Young et al. show similar lattice contraction at similar temperatures, also finding after 10,000 h that contraction increases with increasing temperature (*i.e.,* 475 > 418 > 373 > 333 °C) [9].

Figure 3 (b) shows the Ni_2Cr ordered precipitate size after aging at the different time and temperature combinations. The results show a general increase in Ni_2Cr precipitate size with aging time and temperature (*i.e.,* 475 > 418 > 373 °C). At 475 °C the precipitate size increases from 12nm at 1,000 h to 19nm at 10,000 h. At lower isothermal aging temperatures, the precipitate sizes are smaller in value (compared to the 475 °C) but the phase fraction is similar in Figure 3 (c), suggesting a trade-off between nucleation and growth.

Figure 3 (c) shows the Ni_2Cr phase fraction with time for different isothermal aging temperatures. The results are similar to those in Figure 2 (c), for the off-stoichiometry samples, and plateau around 9%. This suggests the phase fraction relatively insensitive to temperature or composition, within the range explored in this work. At 373 °C at 500 and 1000 h, there is likely some small amount of Ni_2Cr phase present, but it was below the detectable levels of the synchrotron-based XRD.

Figure 3 (d) shows the time- and temperature-dependent evolution of indentation hardness. The changes in indentation hardness at lower temperatures shows similar trends to those given in Figure 2 (d). Rapid hardening again occurs in the first 500 h for both 418 and 475 °C, followed by a gradual increase in hardening with extended aging time. However, at 373 °C where the kinetics of transformation are reduced, there is only a slight change in hardness in the first 1,000 h. Between 1,000 and 3,000 h there is a higher increase in the hardness that gradually increases to 10,000 h, similar to the higher temperature trends. The amount of hardening increases with aging temperature (*i.e.,* 475 > 418 > 373 °C).

A similar correlation between the hardness and precipitate size described in section (3.2) is found here for the (Ni/Cr = 2.0) samples after aging at 373, 418, and 475 °C. Again, the correlation with the phase fraction of the ordered Ni_2Cr phase with the indentation hardness is less apparent, as the lower temperatures phase fraction also appear saturated with further isothermal aging time after the initial detection of Ni_2Cr. Nucleation of the Ni_2Cr phase clearly occurs at early aging times for both 418 and 475 °C. We find these results support that Ni_2Cr is following a diffusion-based growth process [24].

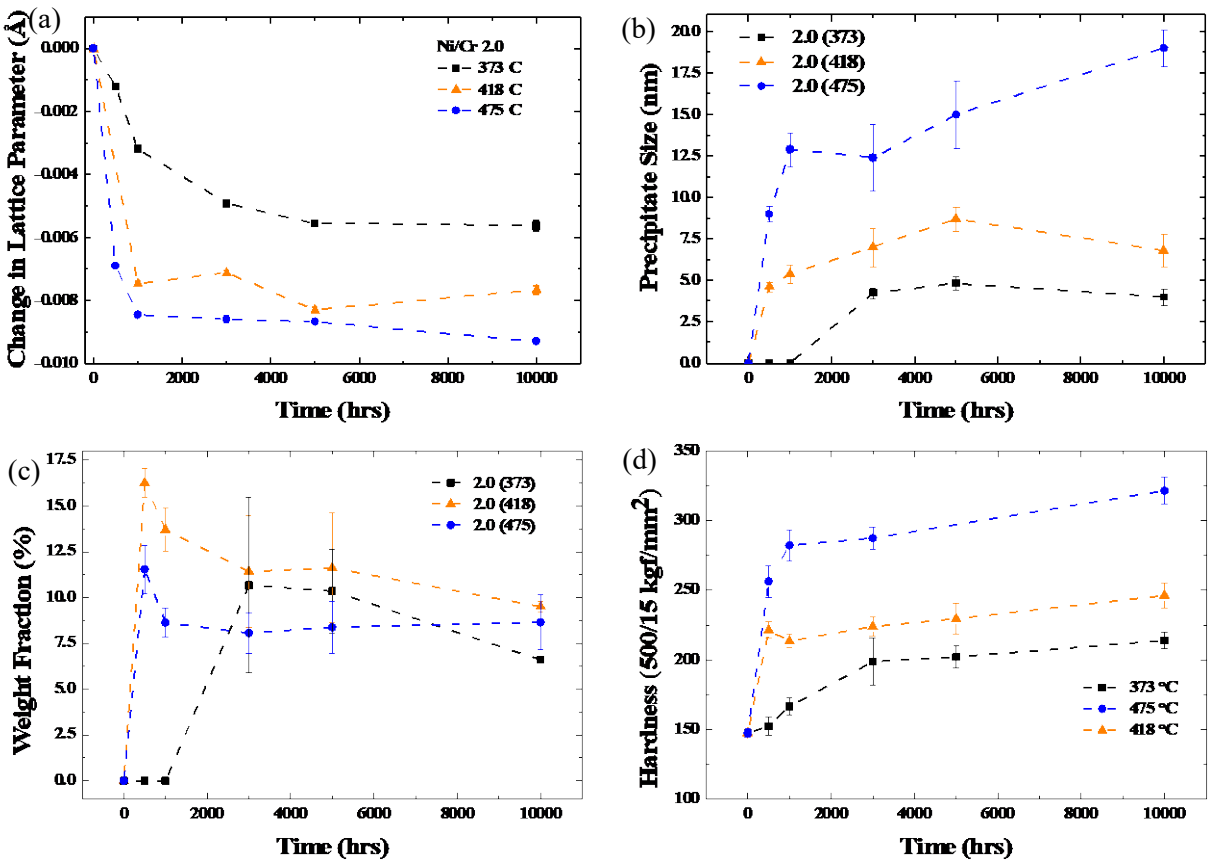

Figure 3. Quantitative XRD and hardness results for the Ni/Cr =2.0 samples as a function of aging time and temperature (a) Change in FCC matrix lattice parameter; (b) Average Ni_2Cr precipitate size; (c) phase fraction of Ni_2Cr phase; (d) Vickers indentation hardness.

3.4. Correlation between Ni_2Cr precipitate size and indentation hardness

The results shown in sections 3.2 and 3.3 highlight that the increase in hardness and Ni_2Cr precipitate size are clearly correlated. To explore this correlation further, the hardness and Ni_2Cr precipitate size are compared in Figure 4. A linear regression with an intercept set to zero was applied to all data (indicating no Ni_2Cr precipitates are present in the AR conditions). The linear relationship of the particle size and hardness is clear, revealing a positive association between the precipitate size of Ni_2Cr and the indentation hardness. This information may potentially be leveraged in future kinetic analysis of Ni_2Cr, where the mechanical performance and material property degradation of commercial Ni-Cr alloys in elevated thermal environments can be better understood based on the average Ni_2Cr precipitate size.

Previous studies have applied KJMA analysis to measured changes in material properties (*i.e.,* hardness [4], [9], [14], lattice contraction [9], [11]) to describe the evolution of Ni_2Cr. A critical assumption in these past KJMA studies was the phase fraction of Ni_2Cr was directly compared to the change in material property, or the material property change is then directly related to the amount of transformation that has occurred in the alloy. Our results here are in contrast to these studies and illustrate that the phase fraction of Ni_2Cr does not correlate as strongly with material property changes (*e.g.,* hardness, which correlates linearly with yield strength [10] and precipitate size) in these Ni-Cr model alloys. Furthermore, our results show that the phase fraction of Ni_2Cr saturates after early aging times, while the hardness continues to

increase with aging times reached in this research. Future analysis should consider use of the precipitate size for characterizing the development of Ni_2Cr and its impact on mechanical properties. A limitation in using the precipitate size over the phase fraction in modified KJMA analysis is when the evolution of the Ni_2Cr in Ni-Cr alloys has reached equilibrium. It is not known if further Ni_2Cr precipitate growth is going to continue to transform the material properties outside of the current aging times in this research.

While there has been a number of studies on the kinetics of Ni_2Cr formation [4], [8], [9], [11], [23], there is also a need to combine with research on the precipitation strengthening mechanisms of Ni_2Cr. It has been established that the size of precipitates has a direct correlation with dislocation motion. A critical resolved shear stress (CRSS) is commonly employed to describe weak or strong coupled dislocations cutting or shearing through precipitates [38]–[41]. Due to the small size of the Ni_2Cr precipitates, we apply a critical resolved shear stress model of weakly coupled dislocations for precipitation hardening, shown in equation (3). In equation (3), τ_{CRSS}, is the critical resolved shear stress, Γ is the anti-phase boundary energy, b is the burger's vector, d is the precipitate diameter (precipitate size of Ni_2Cr), f is the volume fraction, T is the line tension of the dislocation, shown as equation (4) [38], where G is the shear modulus. The shear modulus, G, is calculated from equation (5), where E is the modulus of elasticity, and v is Poisson's ratio. The numerical factor, A, describes the morphology of precipitates and is 0.72, based on the assumption the Ni_2Cr precipitates are spherical [42].

$$\Delta\tau_{CRSS} = \frac{1}{2}\left(\frac{\Gamma}{b}\right)^{\frac{3}{2}}\left(\frac{bdf}{T}\right)^{\frac{1}{2}}A - \frac{1}{2}\left(\frac{\Gamma}{b}\right)f \quad (3)$$

$$T = \frac{1}{2}Gb^2 \quad (4)$$

$$G = \frac{1}{2}\frac{E}{(1+\nu)} \quad (5)$$

$$\Delta HardnessValue = 3\sqrt{3}\tau_{CRSS} \quad (6)$$

We then use this model, and the linear relationship found between hardness and yield strength, as previously found in similar Ni-Cr model alloys [10] to be able to predict the hardness from the estimated critical resolved shear stress. This relationship is shown in equation (6) where we apply Tabor's relationship [43] and Von Mises flow rule [44] to calculate the yield strength from the critical resolved shear stress, as done in previous Ni-based alloy research to calculate the change in hardness [33], [37], [38]. We report our values from the results and those of previous Ni-based alloys using CRSS or equivalent precipitate strengthening models based on precipitate shearing in Table 4.

The parameters for our CRSS model use both values from literature, using model alloy values when possible and commercial Ni-based alloys when there is no model data available, and from our results. The anti-phase boundary energy is from molecular dynamics in model Ni-Cr alloys and is 0.139 [J / m^2] [5]. The burger's vector is from literature on Ni-based alloys and is 0.254 [nm] [33], [37]. The particle diameter is assumed to be the average precipitate size of Ni_2Cr from our work, which we plot on the x-axis of Figure 4. The volume fraction is taken from an average of our results shown in Table 3 for the saturated value. We use a linear assumption with time to account for early increases in volume fraction before reaching the saturated value. The modulus of elasticity is also from literature on Ni-based alloys and taken as 221 [MPa] [40], [46]. The Poisson's ratio is also from literature for Ni-based alloys and taken as 0.35 [40] thus making the shear modulus 81.85 [GPa], which is in close agreement with molecular dynamics simulations [5]. The effectiveness of the CRSS model provides further evidence that the size of Ni_2Cr precipitates has notable impacts on the mechanical properties of Ni-Cr alloys.

Table 4. Values from this study using the critical resolved shear stress for precipitate hardening model of weakly coupled dislocations for gamma prime precipitation.

Parameter	Unit	Model Value	Note
Γ	Jm^{-2}	0.139	Molecular dynamics of model alloy [5]
b	nm	0.254	Ni-based commercial alloy [39], [42]
f	%	9*	This work
E	MPa	221	Ni-based commercial alloy [40], [46]
ν	-	0.35	Ni-based commercial alloy [40]
A	-	0.72	Ni-based commercial alloy [42]
d	nm	varies	This work

* Saturated value.

The CRSS model from equations (1) and (4) is shown as a solid gray line in Figure 4. The model shows good agreement with the experimental measurements in capturing both the change in hardness and precipitate size in Ni-Cr model alloys. The fit of the model could be marginally improved by fitting the parameters directly to the data instead of using existing independent values in the literature, *e.g.* the anti-phase boundary energy could be experimentally refined to the data. However, the agreement of the model, shown in our research, with the molecular dynamics results supports previous literature findings in understanding the deformation behaviors in Ni-based alloys. Our matching experimental results adds confidence to the molecular dynamics simulation with macroscopic material behavior and microstructure observation presented in this research that go beyond the boundary of the recent performed simulations. Additionally, there could be minor improvements to the model if the young's modulus and Poisson's ratio were explicitly known for these specific alloys. However, the values used are representative of Ni-based alloys. Further minor improvements could be made to the linear assumption in volume fraction before reaching the saturated value, however this data is limited in the literature, would not improve the fit of our current data where the volume fraction is considered saturated, and is not accessible in our data sets, *i.e.* requires aging time points between 0 and 500 h for higher temperatures.

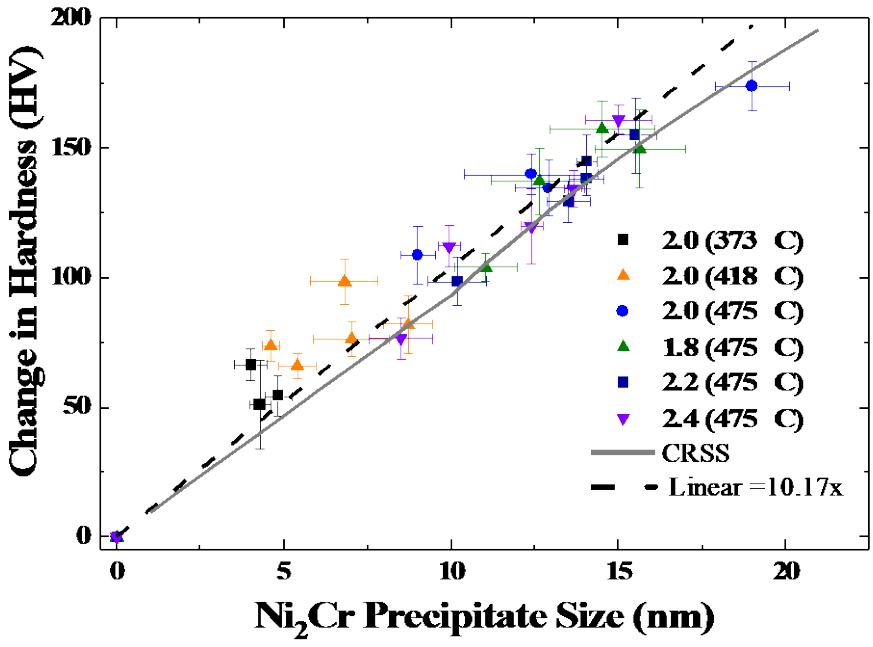

Figure 4. Ni_2Cr precipitate size versus change in hardness. Dashed black line shows linear fit to data. Solid gray line shows the critical resolved shear stress precipitation hardening model of weakly coupled dislocations

4. Conclusion

The development of the Ni_2Cr precipitate phase was investigated in four model Ni-Cr alloys (Ni/Cr = 1.8, 2.0, 2.2, 2.4) isothermally aged at 475 °C for up to 10,000 h. The Ni_2Cr precipitates were also investigated in (Ni/Cr =2.0) alloys isothermally aged at 373, 418, and 475 °C for up to 10,000 h. Results from hardness testing and synchrotron-based XRD were combined to systematically investigate the evolution in hardness and microstructure (Ni_2Cr phase fraction, Ni_2Cr precipitate size, and FCC host lattice contraction) with time, temperature and composition. We find that after 500 h of isothermal aging at 475°C, all stoichiometries show clear Ni_2Cr XRD peaks indicating that Ni_2Cr can form in a wide range of compositions. At lower temperatures, the Ni/Cr=2.0 samples show temperature dependent Ni_2Cr formation, with Ni_2Cr precipitates quantified after 500 h when aged at 418 °C, but not until 3,000 h at 373 °C. We find these results support that Ni_2Cr is following a diffusion based growth process. The Ni_2Cr phase fraction was found to saturate after early aging times to a value around 9 wt.% for all stoichiometries and aging temperatures. We additionally show that there is a clear correlation between the average precipitate size and the change in indentation hardness. This was explained with the critical resolved shear stress model of precipitation hardening with weakly coupled dislocations. We believe this model is able to capture the mechanical behavior changes and estimate the impact on the yield strength from the development of Ni_2Cr in Ni-Cr model alloys based on the precipitate size, which follow a diffusion-controlled growth process. These findings highlight the importance of using advanced characterization techniques sensitive to the minor phase populations and capable of quantifying microstructure.

Acknowledgements

The authors wish to acknowledge Dr. Fei Teng for the foundational work he performed in this area [4]. This research is being supported by the National Science Foundation under Grant no. 1653123-DMR. This publication is also based upon work previously supported by DOE Office of Nuclear Energy's Nuclear Energy University Program, Cooperative Agreement Number DE-NE0008423. The XRD experiments were supported by the U.S. Department of Energy, Office of Nuclear Energy under DOE Idaho Operations Office Contract DEAC07- 051D14517 as part of a Nuclear Science User Facilities rapid turnaround experiment project number (#18-1547). This research utilized resources from the X-ray Powder Diffraction beamline at National Synchrotron Light Source-II, a U.S. Department of Energy (DOE) Office of Science User Facility operated for the DOE Office of Science by Brookhaven National Laboratory under Contract No. DE-SC0012704.

Data Availability

The raw data required to reproduce these findings are available by request from the corresponding author. The processed data required to reproduce these findings are available by request from the corresponding author.

References

[1] M. Song, Y. Yang, M. Wang, W. Kuang, C. R. Lear, and G. S. Was, "Probing long-range ordering in nickel-base alloys with proton irradiation," *Acta Mater*, vol. 156, pp. 446–462, Sep. 2018, doi: 10.1016/j.actamat.2018.06.043.

[2] L. Hao, A. Ruban, and W. Xiong, "CALPHAD modeling based on Gibbs energy functions from zero kevin and improved magnetic model: A case study on the Cr–Ni system," *CALPHAD*, vol. 73, Jun. 2021, doi: 10.1016/j.calphad.2021.102268.

[3] W. Xiong, *Thermodynamic and kinetic investigation of the Fe-Cr-Ni system driven by engineering applications*. Industrial Engineering and Management, Royal Institute of Technology (KTH), 2012.

[4] F. Teng, D. J. Sprouster, G. A. Young, J. H. Ke, and J. D. Tucker, "Effect of stoichiometry on the evolution of thermally annealed long-range ordering in Ni–Cr alloys," *Materialia (Oxf)*, vol. 8, Dec. 2019, doi: 10.1016/j.mtla.2019.100453.

[5] H. T. Vo *et al.*, "Deformation twinning versus slip in Ni-based alloys, containing Pt2Mo-structured, Ni2Cr-typed precipitates," *Mater Des*, vol. 207, Sep. 2021, doi: 10.1016/j.matdes.2021.109820.

[6] N. Aerne, F. Teng, and J. D. Tucker, "Effect of isothermal aging on Ni-Cr-based commercial alloys," 2019.

[7] S. Kim, "Order-disorder reaction in Ni2Cr alloy," in *Transactions of the Korean Nuclear Society Autumn Meeting Gyeongju, Korea*, 2009, vol. 313.

[8] F. Delabrouille, D. Renaud, F. Vaillant, and J. Massoud, "Long range ordering of Alloy 690," 2009.

[9] G. A. Young, J. D. Tucker, and D. R. Eno, "The kinetics of long range ordering in Ni-Cr and Ni-Cr-Fe alloys," in *Proceedings of the 16th Annual Conference on the Environmentally Assisted Cracking of Materials in Nuclear Power Systems-Water Reactors*, 2013, pp. 1–22.

[10] G. A. Young and D. R. Eno, "Long range ordering in model Ni-Cr-X alloys," in *Proceedings of the International Symposium Fontevraud*, 2014, vol. 8, pp. 14–18.

[11] A. Marucco, "Atomic ordering in the Ni-Cr-Fe system," *Materials Science and Engineering: A*, vol. 189, no. 1–2, pp. 267–276, 1994.
[12] A. Verma, J. B. Singh, S. D. Kaushik, and V. Siruguri, "Lattice parameter variation and its effect on precipitation behaviour of ordered Ni2(Cr,Mo) phase in Ni-Cr-Mo alloys," *J Alloys Compd*, vol. 813, Jan. 2020, doi: 10.1016/j.jallcom.2019.152195.
[13] B. Stephan, D. Jacob, F. Delabrouille, and L. Legras, "A kinetic study of order-disorder transition in Ni–Cr based alloys," in *Minerals, Metals and Materials Series*, 2018, vol. Part F9, pp. 233–249. doi: 10.1007/978-3-319-67244-1_15.
[14] B. Gwalani *et al.*, "Experimental investigation of the ordering pathway in a Ni-33 at.% Cr alloy," *Acta Mater*, vol. 115, pp. 372–384, 2016.
[15] T. Allen, J. Busby, M. Meyer, and D. Petti, "Materials challenges for nuclear systems," *Materials today*, vol. 13, no. 12, pp. 14–23, 2010.
[16] S. J. Zinkle and G. S. Was, "Materials challenges in nuclear energy," *Acta Mater*, vol. 61, no. 3, pp. 735–758, Feb. 2013, doi: 10.1016/j.actamat.2012.11.004.
[17] G. S. Was, *Fundamentals of radiation materials science: metals and alloys*. springer, 2016.
[18] G. A. Young *et al.*, "Effect of long range order on the stress corrosion susceptibility of a nickel-33 at% chromium alloy," *Corrosion*, vol. 72, no. 11, pp. 1433–1437, 2016.
[19] A. N. Kolmogorov, "On the statistical theory of the crystallization of metals," *Bull. Acad. Sci. USSR, Math. Ser*, vol. 1, no. 3, pp. 355–359, 1937.
[20] M. Avrami, "Kinetics of phase change. II transformation-time relations for random distribution of nuclei," *J Chem Phys*, vol. 8, no. 2, pp. 212–224, 1940.
[21] M. Avrami, "Granulation, phase change, and microstructure kinetics of phase change. III," *J Chem Phys*, vol. 9, no. 2, pp. 177–184, 1941.
[22] W. A. Johnson, "Reaction kinetics in processes of nucleation and growth," *Am. Inst. Min. Metal. Petro. Eng.*, vol. 135, pp. 416–458, 1939.
[23] L. Barnard *et al.*, "Atomistic modeling of the order–disorder phase transformation in the Ni2Cr model alloy," *Acta Mater*, vol. 81, pp. 258–271, 2014.
[24] J.-H. Ke, G. A. Young, and J. D. Tucker, "Ab initio study of phosphorus effect on vacancy-mediated process in nickel alloys–An insight into Ni2Cr ordering," *Acta Mater*, vol. 172, pp. 30–43, 2019.
[25] J. M. Schneider, M. Bigerelle, and A. Iost, "Statistical analysis of the Vickers hardness," *Materials Science and Engineering A*, vol. 262, no. 1–2, pp. 256–263, Apr. 1999, doi: 10.1016/s0921-5093(98)01000-4.
[26] X. Shi, S. Ghose, and E. Dooryhee, "Performance calculations of the X-ray powder diffraction beamline at NSLS-II," *J Synchrotron Radiat*, vol. 20, no. 2, pp. 234–242, 2013.
[27] D. J. Sprouster *et al.*, "Advanced synchrotron characterization techniques for fusion materials science," *Journal of Nuclear Materials*, vol. 543, Jan. 2021, doi: 10.1016/j.jnucmat.2020.152574.
[28] J. Ilavsky, "Nika: software for two-dimensional data reduction," *J Appl Crystallogr*, vol. 45, no. 2, pp. 324–328, 2012.
[29] J. Ilavsky and P. R. Jemian, "Irena: tool suite for modeling and analysis of small-angle scattering," *J Appl Crystallogr*, vol. 42, no. 2, pp. 347–353, 2009.
[30] L. Lutterotti, M. Bortolotti, G. Ischia, I. Lonardelli, and H.-R. Wenk, "Rietveld texture analysis from diffraction images," in *Tenth European Powder Diffraction Conference*, 2015, pp. 125–130.
[31] I. C. Madsen, N. V. Y. Scarlett, L. M. D. Cranswick, and T. Lwin, "Outcomes of the International Union of Crystallography Commission on Powder Diffraction Round Robin on Quantitative Phase Analysis: samples 1 a to 1 h," *J Appl Crystallogr*, vol. 34, no. 4, pp. 409–426, Aug. 2001, doi: 10.1107/S0021889801007476.
[32] H. Borchert *et al.*, "Determination of nanocrystal sizes: A comparison of TEM, SAXS, and XRD studies of highly monodisperse CoPt 3 particles," *Langmuir*, vol. 21, no. 5, pp. 1931–1936, Mar. 2005, doi: 10.1021/la0477183.

[33] R. J. Hill and C. J. Howard, “Quantitative Phase Analysis from Neutron Powder Diffraction Data Using the Rietveid Method,” 1987.
[34] R. E. Dinnebier and S. J. L. Billinge, *Powder diffraction: theory and practice*. Royal society of chemistry, 2008.
[35] J. D. Tucker, “AB INITIO-BASED MODELING OF RADIATION EFFECTS IN THE NI-FE-CR SYSTEM,” 2008.
[36] L. Vegard, “Die konstitution der mischkristalle und die raumfüllung der atome,” *Zeitschrift für Physik*, vol. 5, no. 1, pp. 17–26, 1921.
[37] P. Nash, “Phase diagrams of binary nickel alloys,” *ASM International(USA), 1991,* p. 394, 1991.
[38] L. M. Brown and R. K. Ham, “Strengthening methods in crystals,” *Applied Science, London*, vol. 9, 1971.
[39] Q. Wang, Z. Li, S. Pang, X. Li, C. Dong, and P. K. Liaw, “Coherent precipitation and strengthening in compositionally complex alloys: A review,” *Entropy*, vol. 20, no. 11. MDPI AG, Nov. 01, 2018. doi: 10.3390/e20110878.
[40] J. H. Oh, I. C. Choi, Y. J. Kim, B. G. Yoo, and J. il Jang, “Variations in overall- and phase-hardness of a new Ni-based superalloy during isothermal aging,” *Materials Science and Engineering A*, vol. 528, no. 19–20, pp. 6121–6127, Jul. 2011, doi: 10.1016/j.msea.2011.03.115.
[41] J. Moon, S. Kim, J. il Jang, J. Lee, and C. Lee, “Orowan strengthening effect on the nanoindentation hardness of the ferrite matrix in microalloyed steels,” *Materials Science and Engineering A*, vol. 487, no. 1–2, pp. 552–557, Jul. 2008, doi: 10.1016/j.msea.2007.10.046.
[42] B. Reppich, “Some new aspects concerning particle hardening mechanisms in γ’ precipitating Ni-base alloys—I. Theoretical concept,” *Acta Metallurgica*, vol. 30, no. 1, pp. 87–94, Jan. 1982, doi: 10.1016/0001-6160(82)90048-7.
[43] D. Tabor, “A simple theory of static and dynamic hardness,” *Proc R Soc Lond A Math Phys Sci*, vol. 192, no. 1029, pp. 247–274, 1948.
[44] R. v Mises, “Mechanik der festen Körper im plastisch-deformablen Zustand,” *Nachrichten von der Gesellschaft der Wissenschaften zu Göttingen, Mathematisch-Physikalische Klasse*, vol. 1913, pp. 582–592, 1913.
[45] P. Zhang, S. X. Li, and Z. F. Zhang, “General relationship between strength and hardness,” *Materials Science and Engineering A*, vol. 529, no. 1, pp. 62–73, Nov. 2011, doi: 10.1016/j.msea.2011.08.061.
[46] J. James, J. Julian, J. Rahul, G. Philip, J. Devassy, and P. Reba, “Effect of recasting on physical properties of base metal alloys: An in vitro study,” *J Int Soc Prev Community Dent*, vol. 8, no. 5, p. 457, 2018, doi: 10.4103/jispcd.jispcd_237_18.

Supplemental material

The figures presented as supplemental material help to show: an example of the entire XRD patterns, the (Ni/Cr=2.0) patterns at 1000 h at all temperatures to show in detail the timepoint before detection of Ni_2Cr at temperature 373 °C, the same time point for all stoichiometries at 475 °C for comparison, the evolution of patterns collected for (Ni/Cr=2.0) at 373 and 418 °C, and finally AR patterns to show there is no Ni_2Cr detected before the isothermal aging campaigns. These AR specimens were not rotated during collection, and taken at a different time, with different beamline conditions, thus the FCC peaks are shifted with different intensities.

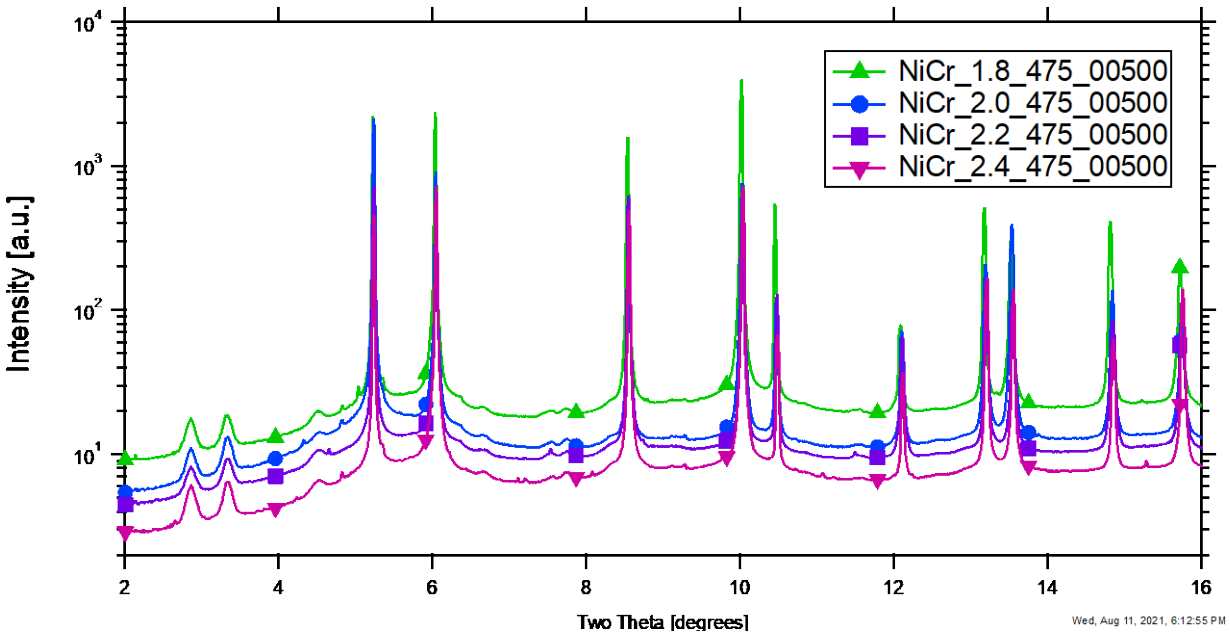

Figure S1. Example of the entire XRD patterns from isothermal aging at 475 °C for 500 h.

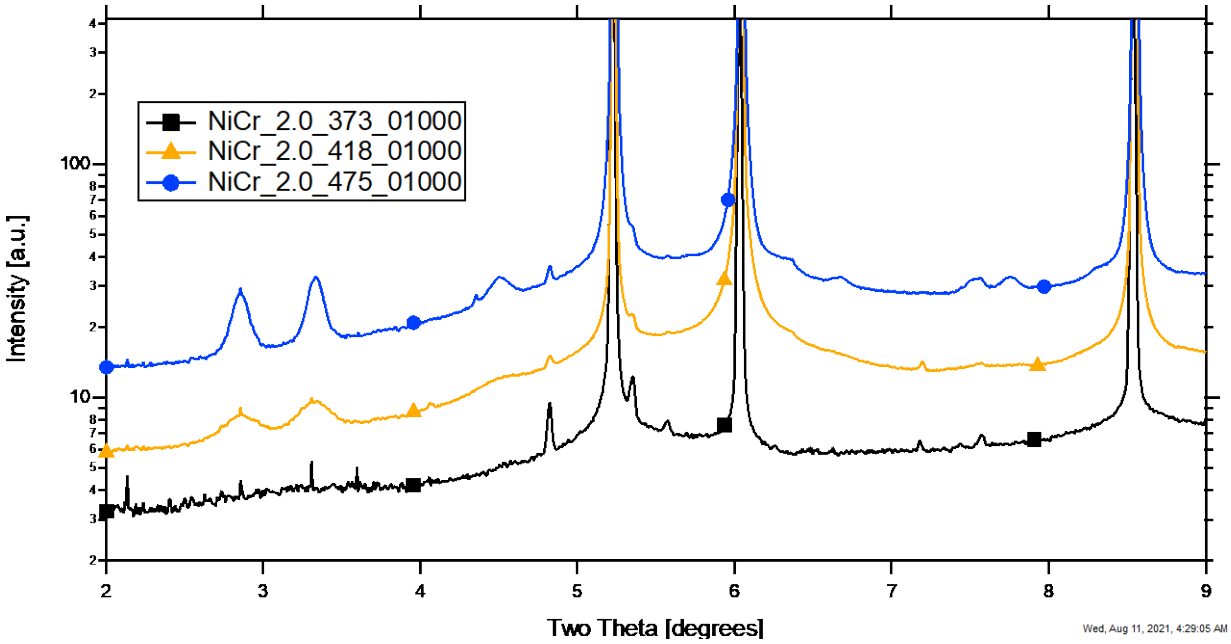

Figure S2. XRD patterns of Ni/Cr=2.0 sample from all isothermal aging temperatures at 1000 h.

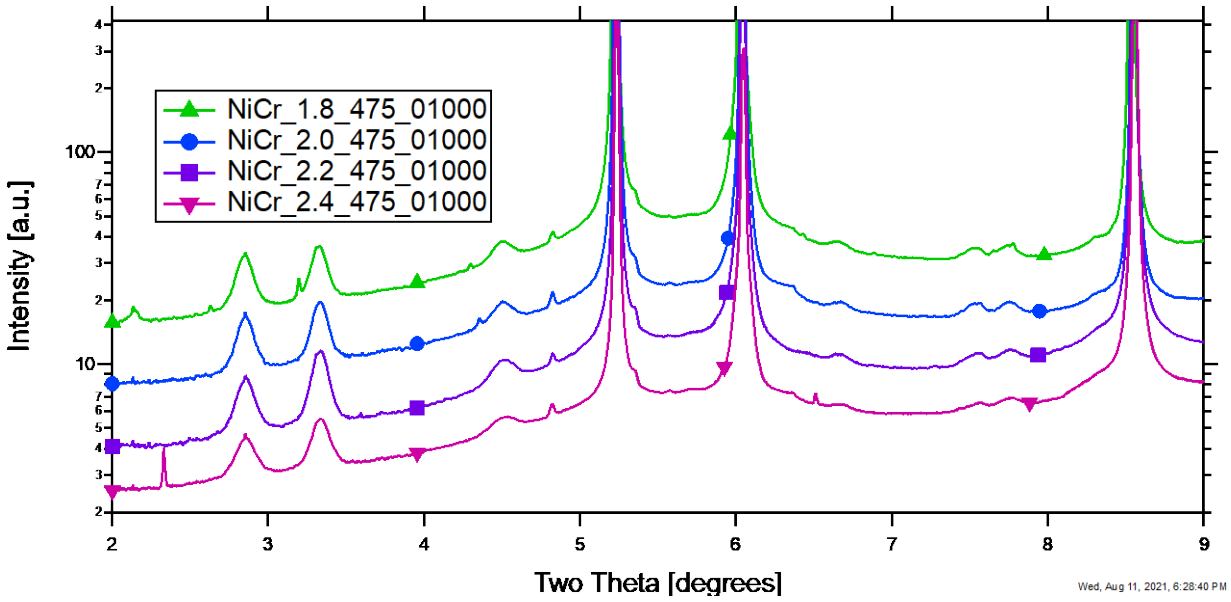

Figure S3. XRD patterns of all stoichiometries from isothermal aging at 475 °C for 1000 h.

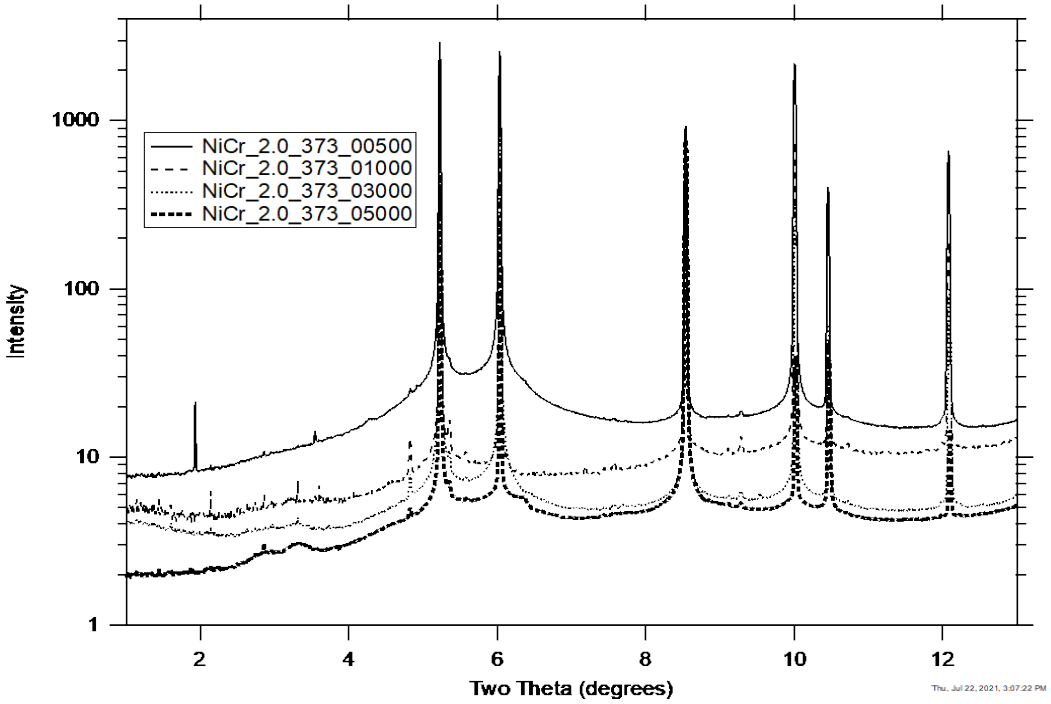

Figure S4. XRD patterns of stoichiometric Ni/Cr=2.0 sample at isothermal aging 373 °C after aging from top pattern downward 500, 1000, 3000, and 5000 h.

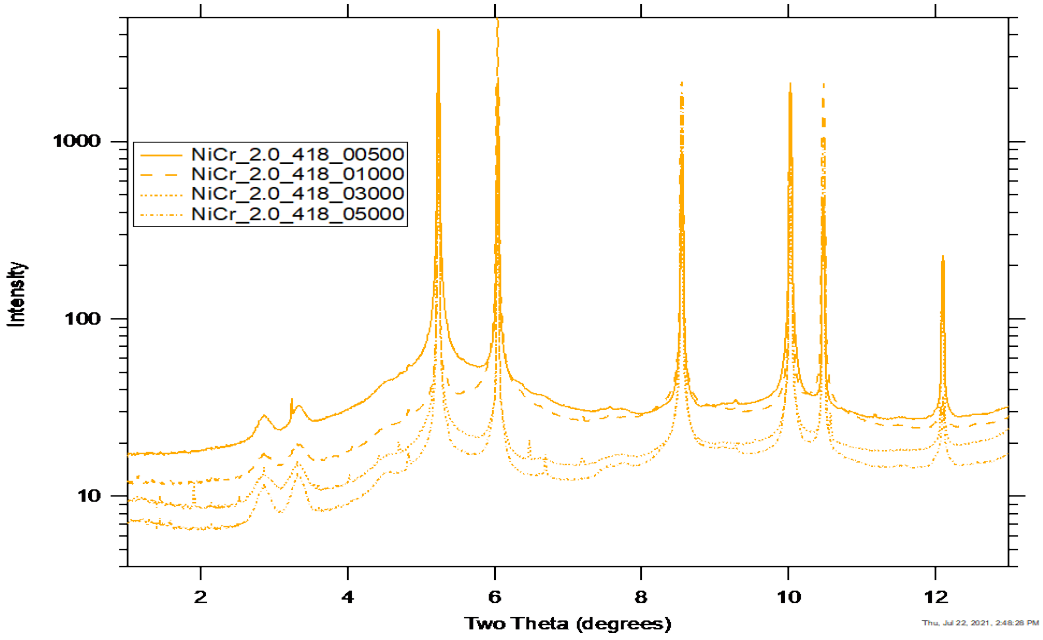

Figure S5. XRD patterns showing evolution of isothermal aging at 418 °C from stoichiometric Ni/Cr=2.0 from top pattern downward 500, 1000, 3000, and 5000 h.

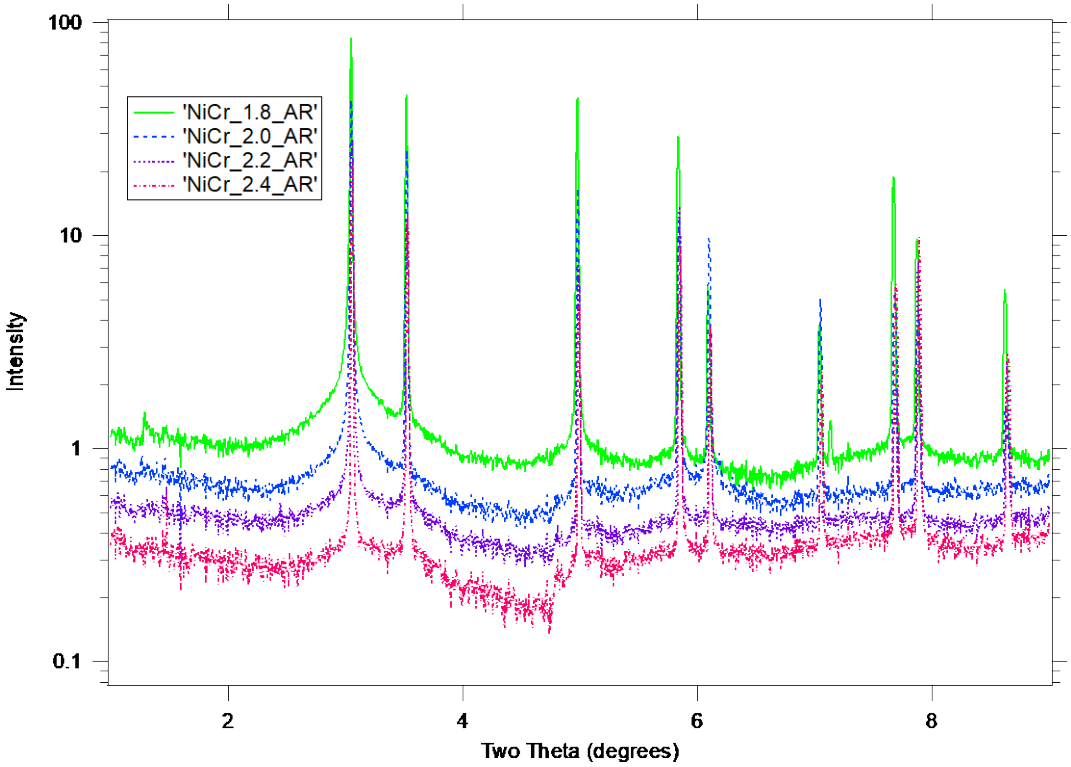

Figure S61. XRD patterns of AR samples from all stoichiometries.